Dynamics of a Xe cluster plasma produced by an intense ultrashort pulse KrF laser

G. M. Petrov, J. Davis, A. L. Velikovich, P. Kepple, A. Dasgupta, and R. W. Clark
Naval Research Laboratory, Plasma Physics Division, 4555 Overlook Avenue SW, Washington, DC 20375

(Received 28 February 2005; accepted 19 April 2005; published online 2 June 2005)

The dynamics of Xe clusters with initial radius between 10 and 100 Å irradiated by an IR subpicosecond laser pulse is investigated. The evolution of the cluster is modeled with a relativistic time-dependent three-dimensional particle simulation model. The focus of this investigation is to understand the energy absorption of clusters and how the absorbed energy is distributed among the various degrees of freedom. The consequence of the initial cluster radius on the absorbed energy, average charge per atom, mean electron and ion energies, ionization, removal of electrons from the cluster, and cluster expansion was studied. The absorbed energy per cluster scales as $N^{5/3}$, and the mean electron and ion energies scale as $N^{1/3}$ and $N^{2/3}$, respectively (N is the number of atoms per cluster). A significant fraction of the absorbed energy ($\sim$90%) is converted into kinetic energy with comparable contribution to electrons and ions. The energy balance suggests that smaller clusters are more efficient as radiators, while larger clusters are more conducive to particle acceleration. The radiation yield of clusters with initial radius 20–50 Å irradiated by a laser with peak intensity 10^{16} W/cm^2 is determined to be 1%–2%. © *2005 American Institute of Physics*.
[DOI: 10.1063/1.1928367]

I. INTRODUCTION

The last several years have witnessed an explosion of activity involving the interaction of clusters with intense ultrashort pulse lasers.[1–3] The interest in laser-cluster interaction has not only been academic but also directed at a wide variety of potential applications. Clusters can be used to generate a compact source of incoherent as well as coherent x rays,[4] and fast ions capable of driving a fusion reaction in a deuterium plasma.[1,2] Some of the potential applications include extreme ultraviolet (EUV) lithography, EUV and x-ray microscopy, x-ray tomography, and a variety of applications in biological and material sciences. One of the first self-consistent models, the so-called "nanoplasma model,"[5] treated the cluster as a miniature (few nanometers in size) high-density spherical plasma. Although this model attempted to capture the main features of the laser-cluster interaction, it was essentially a spatially averaged fluid model. Later on, others suggested improvements or developed similar zero-dimensional or one-dimensional fluid models.[6,7] The fluid model had limited success in explaining some of the observations, however, it left much to be desired. Another way of studying the cluster dynamics is to employ a particle simulation model, in order to avoid potential problems of fluid modeling (such as the finite size of the cluster and the relatively small number of particles). Particle models can capture some unique features of the cluster, such as the location of particles and their velocities. In a three-dimensional version, particle simulation models can provide a detailed quantitative description of the cluster. A number of molecular dynamics models emerged in the literature during the last few years, studying different aspects of laser-cluster interaction.[8–17]

In our previous paper[17] we developed a relativistic time-dependent three-dimensional (3D) particle-particle simulation model to study the interaction of an intense ultrashort pulse KrF laser with Xe clusters with initial radius of 20 Å. The model was based upon following the trajectories of electrons and ions according to the relativistic equations of motion. Instead of particle-mesh interpolation we implemented direct particle-particle interactions. Thus, we managed to avoid both the interpolation of charges onto a two- or three-dimensional grid and the solution of the Poisson equation as in conventional particle-in-cell (PIC) schemes. The lack of a grid, in particular, makes our approach simple and very robust. So far we have not encountered any problems of a numerical nature, such as instabilities or oscillations. The model was applied to the study of Xe clusters subject to ultrahigh laser intensities ranging from 10^{17} to 10^{21} W/cm^2. The details of the electron and ion motions, removal of electrons from the cluster, and power absorption as the cluster evolves in time were investigated. In particular, we explored the behavior of the cluster in the relativistic domain at laser intensities of 10^{20} W/cm^2, sufficient to transition to the so-called "collective oscillation model." We found that at these extreme laser intensities the magnetic field has a profound effect upon the shape and trajectory of the electron cloud. The electrons are accelerated to relativistic velocities in the direction of laser propagation, and the magnetic field distorts the shape of the electron cloud in a form of a pancake. At peak laser intensities between 10^{17} and 10^{20} W/cm^2, all free electrons are promptly removed from the cluster and form a plasma. From this study we also concluded that the laser-cluster interaction at laser intensities exceeding 10^{17} W/cm^2 is a three-dimensional problem and must be treated accordingly.

Our earlier study[17] covered the domain of high laser intensities, sufficient to drive all free electrons out of the clus-

ter on a very short time scale, of the order of a few femtoseconds. In the opposite case of moderate peak laser intensities ($\sim 10^{16}$ W/cm^2) the laser electric field is comparable to the field created by the charge separation of electrons and ions, and the cluster properties are a result of complex interplay between peak laser intensity and cluster size. Most electrons are trapped inside the cluster due to strong Coulomb attraction to the ion core. The high electron and ion densities inside the cluster open new channels of elementary processes, such as collisional ionization and recombination. The nature of the interactions between the particles switches from "collisionless" to collisional. As a consequence, the power absorption through inverse bremsstrahlung is expected to grow with the cluster size due to the collisional nature of the interactions. Thus the domain of low to moderate laser intensities ($\leqslant 10^{16}$ W/cm^2) is even more challenging, as the cluster properties are more difficult to predict. We address these and other issues using particles simulations. This technique is well suited to study some elusive features of the laser-cluster interaction such as the electron energy distribution function (EEDF), the ion energy distribution function (IEDF), positions of particles both inside and outside the cluster, removal of electrons from the cluster and resonance absorption. But the greatest advantage of the particle simulation technique is its capability to study objects in two and three dimensions. The present work is devoted to study the interaction of Xe clusters of various sizes with an ultrashort pulse laser at moderate peak intensity ($\sim 10^{16}$ W/cm^2) by a molecular dynamics model.

In this paper we want to distinguish the differences between small and large clusters in terms of the way they absorb energy and how that energy is distributed among different channels. Knowledge of the latter is crucial for applications such as particle acceleration, fusion, and x-ray generation. Part of the energy absorbed by the cluster is through optical field ionization (OFI) and the rest of the energy ends up as kinetic and potential energies of electrons and ions. It is instructive to know how the absorbed energy depends on the cluster size. Another objective is to provide general recommendations for matching cluster size and laser intensity depending on applications. It is of fundamental importance to predict whether clusters with particular properties are better for radiation production or for particle acceleration, and to select clusters with properties (such as cluster size and number of atoms) most favorable for a particular application. In this study we will determine the cluster size that optimizes radiation.

II. MODEL ASSUMPTIONS

We employed the molecular dynamics model developed in Ref. 17 to study the dynamics of Xe clusters with different number of atoms irradiated by a subpicosecond laser with wavelength $\lambda = 800$ nm at a peak laser intensity $I_0 = 10^{16}$ W/cm^2. In all calculations the laser intensity pulse shape, shown in Fig. 1(a), has a Gaussian profile $I(t) = I_0 \exp[-(t-t_0)^2/\tau^2]$ with parameters $t_0 = 200$ fs and $\tau = 75$ fs. These conditions are similar to that in Ref. 5. The electromagnetic wave direction of propagation is along the y axis, the laser electric and magnetic fields are parallel to the x and z axes, respectively, i.e., $E = [E_x(t), 0, 0]$ and $B = [0, 0, B_z(t)]$. The laser electric field strength is taken to be of the form $E_x(t) = E_0(t)\cos(\omega t)$ with amplitude expressed by the laser intensity according to $E_0(t) = \sqrt{8\pi I(t)/c}$, where c is the speed of light. The attenuation of the laser field inside the cluster is neglected (large skin depth), as well as "ignition effects" (local increase or decrease of the laser field due to the inner field generated by charged particles). The combined action of the laser and inner field has been discussed in Ref. 8.

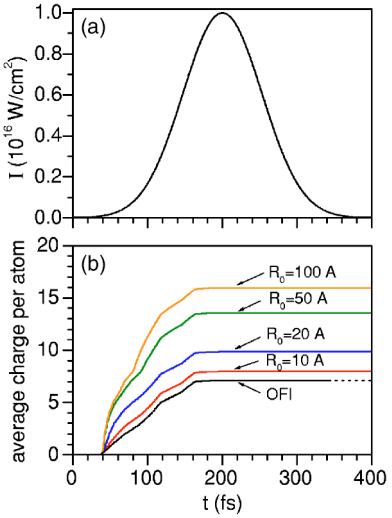

FIG. 1. (Color online) Laser intensity vs time (a) and average charge per atom $Z-1$ for clusters with initial cluster radius $R_0 = 10$, 20, 50, and 100 Å (b). Dot line: average charge per atom to OFI [formula (1a) in Ref. 17]. The laser wavelength is $\lambda = 800$ nm. For $R_0 = 10$ Å, the computations are carried out with 49 ion macroparticles with charge $qn = [Z(t)-1]e_0$ and 392 electron macroparticles with charge $qn = -e_0$ (e_0 is the absolute value of the electron charge); for $R_0 = 20$ Å, we use 100 ion macroparticles with charge $qn = 3.93[Z(t)-1]e_0$ and 776 electron macroparticles with charge $qn = -5e_0$; for $R_0 = 50$ Å, 100 ion macroparticles with charge $qn = 61.44[Z(t)-1]e_0$ and 835 electron macroparticles with charge $qn = -100e_0$; for $R_0 = 100$ Å, 100 ion macroparticles with charge $qn = 491.5[Z(t)-1]e_0$ and 784 electron macroparticles with charge $qn = -1000e_0$. The integration time step is 6×10^{-19} s ($\sim$5000 steps per laser cycle).

We study a single cluster with initial radius R_0 consisting of $N = (R_0\,[\text{Å}]/2.73)^3$ atoms located at the origin of the coordinate system. For clusters with $R_0 < 15$ Å the motion of each electron and ion is followed, but for larger clusters lumping of particles becomes necessary and we use macroparticles. A macroparticle represents n identical particles (atoms, electrons, or ions) with a charge qn and mass mn (q and m are the individual particle charge and mass). Initially the cluster is spherically symmetric and spatially uniform, and consists only of neutral atoms. At time $t = 0$, the beginning of the calculations, $\sim$100 neutral macroparticles, representing these atoms, are put randomly inside a sphere with radius R_0. As time advances, the laser intensity increases and at appropriate intensity the neutral macroparticles are ionized through OFI and attain positive charge. The charged macroparticles then move according to their equations of motion[17] (see the Appendix). Collisional ionization and OFI are accounted for by increasing either the number of macroparticles or their charge. During the computations the number of

ion macroparticles remains the same, but their charge dynamically increases. The electron macroparticles are treated differently: collisional ionization and OFI add new electron macroparticles with a fixed charge. The charge of the electron macroparticles is chosen in advance before the computations begin and it is kept constant throughout the calculations. For example, if it is equal to $NZ(t\rightarrow\infty)/1000$, where $Z(t\rightarrow\infty)-1$ is the expected final average charge per atom [cf. Fig. 1(b)], there will be about a thousand electron macroparticles at the end of the computations. The total number of macroparticles varies in time. Initially there are only about a hundred macroparticles (equal to the number of neutral macroparticles initializing the computations), but their number increases due to ionization in the cluster. The total number of macroparticles is kept around 10^3 in order to prevent excessive computation time, which scales as the number of macroparticles squared.

A large number of macroparticles result in close interactions between them for a prolonged time, and careful handling of the interaction potentials between macroparticles is necessary. We adopted the interaction potentials from Refs. 9 and 10, which describe the Coulomb forces at close encounters. To account for lumping of particles we made a slight modification of the smoothing parameter r_0 of the interaction potential $\Phi_{ij}=q_iq_j/\sqrt{|r_i-r_j|^2+r_0^2}$ between same charge macroparticles i and j. The parameter r_0, which is $\sim$0.2 Å for electrons and $\sim$1 Å for ions,[9] has been replaced by the parameter $r_0\rightarrow r_0n^{1/3}$. This is equivalent to increasing by $n^{1/3}$ times the "size" of a macroparticle containing n electrons or ions. In other words, instead of using point charges as in our previous work,[17] we use finite-size particles as in conventional PIC codes. The constant C of the short-range term of the electron-ion interaction potential $\Phi_{ij}=q_iq_j/|r_i-r_j|+C/|r_i-r_j|^6$ has also been modified so that the potential becomes repulsive at a distance $n^{1/3}$ times larger compared to that arising from the interaction of an electron and an ion. These measures aim to prevent the particle penetration problem,[9,10] as well as the problem, discussed presently. To make the computations manageable we use $\sim10^3$ macroparticles, $\sim10^2$ of which are ions. For the largest cluster considered each macroparticle contains about a thousand particles (electrons or ions). Further increase of the number of electrons/ions per macroparticle n produces a problem. The macroparticle is subject to a force from the electromagnetic field and electrostatic force due to Coulomb interactions with other macroparticles. The former force is proportional to the number of electrons/ions per test particle n, while the latter is proportional to $q^2\sim n^2$. Large $n(n>10^3)$ leads to a numerically stable, but physically meaningless solution, expressed by an excessively large negative potential energy balanced by a positive kinetic energy. That is why the number of particles per macroparticle is limited to about a thousand in order to achieve the correct physical solution. For this reason, we were not able to study clusters with an initial radius larger than 100 Å.

The computational domain is a cube with a side equal to the intercluster distance, which is estimated to be $\sim20R_0$. Periodic boundary conditions are applied at $x,y,z=\pm10R_0$ to account for the impact of neighboring clusters. The periodic boundary conditions imply that any macroparticle that leaves the computational box reappears at the other side of the box.

For the purpose of defining inner and outer electrons, the cluster is assumed to be slowly expanding in time sphere with radius R. The cluster radius is defined as $R(t)=\sqrt{2\Sigma_{p=i}(x_i^2+y_i^2+z_i^2)/N}$, where (x_i,y_i,z_i) are the ith ion coordinates at time t. The summation is over all ions. "Inner electrons," i.e., electrons that reside inside the cluster, are those for which $|r_k|=\sqrt{x_k^2+y_k^2+z_k^2}\leq R(t)$, where $|r_k|$ is the distance of the kth electron to the origin of the coordinate system. Electrons for which $|r_k|>R(t)$ are called "outer electrons."

III. RESULTS AND DISCUSSIONS

Our primary objective is to investigate the impact of the cluster size on specific cluster properties. Clusters with initial radius of $R_0=10$, 20, 50, and 100 Å are studied. Clusters composed of a few hundreds to a thousand atoms were studied in Ref. 8. We are dealing with clusters whose number of atoms varies from 50 to 50 000. Our simulations begin at time $t=0$ with neutral atoms subject to negligibly small laser intensity, which increases in time as shown in Fig. 1(a). For the first $\sim$40 fs the average charge per atom remains zero since the laser intensity is too small to produce a significant number of electrons. When the laser intensity becomes sufficiently high to ionize neutral Xe atoms through OFI, the average charge per atom increases [Fig. 1(b)] and shortly after the laser intensity goes through maximum it levels off. This behavior is independent of the cluster size, except that clusters with different number of atoms have slightly different final average charge per atom. The over-the-barrier ionization would bring the average charge per atom to $Z-1\approx7$ (Fig. 1, dot line).[17] The final average charge per atom depends on the contribution of collisional ionization. Clusters with initial radius $\sim$10 Å tend to lose their inner electrons quickly and the collisional ionization is not effective. As a result these clusters experience only a modest increase in the average charge per atom due to collisional ionization. Large clusters are much more effective in keeping the electrons inside the cluster. Consequently, the role of the collisional ionization increases with R_0. For clusters with initial radius $R_0=100$ Å the collisional ionization contributes equally with the OFI and doubles the average charge per atom. Further increase of the cluster size, beyond $\sim$100 Å, however, may lead to the opposite effect. The cluster will "overheat," i.e., the electrons will acquire a kinetic energy of hundreds of keV, making the collisional ionization rate for low-energy threshold (100–300 eV for $Z=8-15$) negligible. Obviously, there is a trade-off: the cluster must be large enough to retain the electrons inside, but not so large as to cause "overheating." The optimum initial cluster size for achieving the highest charge per atom at this intensity is $R_0\approx10^2$ Å.

The energy absorption by clusters is of paramount importance. The clusters are excellent absorbers of laser energy, a fact that was recognized from the earlier works of laser-cluster interaction, both theoretically and experimentally.[5] We used our molecular dynamics model to assess the energy

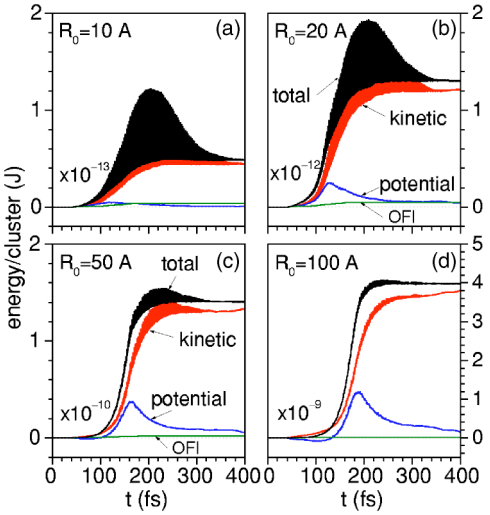

FIG. 2. (Color online) Kinetic, potential, OFI, and total energy per cluster vs time for clusters with initial radius $R_0=10$ Å (a), 20 Å (b), 50 Å (c), and 100 Å (d). The conditions are the same as in Fig. 1.

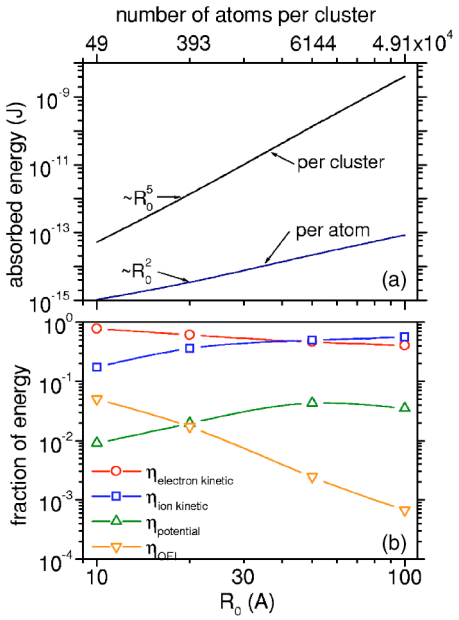

FIG. 3. (Color online) Absorbed energy per cluster and absorbed energy per atom vs initial cluster radius (a). Energy balance (b). The conditions are the same as in Fig. 1.

absorption and its distribution among various degrees of freedom for clusters with different number of atoms. In our previous paper we derived the energy balance equation, which states that the absorbed energy equals the sum of the kinetic and potential energies of all species.[17] In the present study, we extend it by adding the term $E_k^{\mathrm{OFI}}=\Sigma_{m=1}^{Z^{\mathrm{OFI}}(t)}I(m)$, which is the energy per atom spent for OFI. In this expression the summation is over the ionization potentials of all ions starting from neutral Xe up to the ion with average charge per atom $Z^{\mathrm{OFI}}(t)-1$ (Z^{OFI} is defined in Ref. 17). The modified energy balance equation reads

$$\sum_{k=e,i} E_k^{\mathrm{kin}}(t)+\sum_{k=e,i} E_k^{\mathrm{pot}}(t)+\sum_{k=i} E_k^{\mathrm{OFI}}(t)=E^{\mathrm{abs}}(t). \qquad (1)$$

The summation in the first two terms on the left-hand side is over all electrons and ions, while the summation in the third term is only over the ions. The term on the right-hand side is the total energy absorbed in the system. The contribution of different terms to the energy balance (1) versus time for the same four cluster sizes is plotted in Fig. 2. The electrons and ions gain kinetic energy from the laser field due to inverse bremsstrahlung. This energy is slowly increasing in time responding to changes in the laser intensity. The ponderomotive energy adds a high-frequency component to it, which is significant for clusters with initial radius of 10–20 Å [Fig. 2(a)]. With increasing cluster size the "background" energy acquired due to inverse bremsstrahlung increases and the contribution of the high-frequency component diminishes. The potential energy is positive, resulting mostly from charge separation, but it remains significantly smaller than the kinetic energy. The energy spent for OFI is also plotted in Fig. 2. In most cases the energy loss due to OFI is only a small fraction of the absorbed energy, but in some instances, such as small clusters and/or low laser intensity, it can be substantial. Equation (1) does not include energy losses due to scattered radiation, which is negligible, neither losses due to bremsstrahlung radiation in electron-ion collisions. The latter was estimated to be less than 1% of the energy absorption.

A more detailed picture of the energy absorption is given in Fig. 3. The top figure displays the energy absorption per cluster and the energy absorption per atom. The latter is defined as the energy absorbed per cluster divided by N, the number of atoms per cluster. Both values are taken at the end of the laser pulse ($t=400$ fs). The absorbed energy per cluster E^{abs} is a nonlinear function of the initial cluster radius R_0. It scales with R_0 in the same manner as the electrostatic energy of the charged ion core of the cluster, $E_i=Q^2/2C$. $Q=eNZ$ is the total charge of the ion core (assuming that the electron cloud surrounds the core symmetrically and its effect on the core expansion can be therefore neglected), and $C=R_0$ is its capacitance. Since the cluster radius scales as $R_0\sim N^{1/3}$, we find that $E_i\sim N^{5/3}$. Indeed, a power fit made to the upper curve in Fig. 3 reveals the same dependence. As the ion core of the cluster expands, this potential energy is eventually transformed into the kinetic energy of the ions, which therefore scales with the cluster size as $N^{5/3}\sim R_0^5$ ($N^{2/3}$ per ion). In contrast with the ions, the electrons always feel the electrostatic field of the ion core, whose charge exactly equals that of the electron cloud. Therefore, the electrons move in a dipole charge distribution, whose capacitance is proportional to $N^{2/3}\sim R_0^2$. Due to the virial theorem, the time-averaged kinetic energy of the electrons oscillating in a finite spatial domain is proportional to their time-averaged potential energy, which scales as $Q^2/2C\sim N^{4/3}\sim R_0^4$ ($N^{1/3}$ per electron).

A more intuitive quantity for comparison is the absorbed energy per atom. Since the number of atoms per cluster scales as $N\sim R_0^3$, the absorbed energy per atom is proportional to $E^{\mathrm{abs}}/N\sim R_0^2\sim N^{2/3}$. This confirms that grouping, i.e., the number of atoms per cluster, is directly linked to the

power absorption and explains why clusters absorb more energy than gases. Further details are given in Fig. 3(b), detailing how the absorbed energy is distributed into different channels. The absorbed energy is spent for OFI for increasing the kinetic energy of electrons and ions, and some remains in the system as potential energy. One may expect that the predominant part of the absorbed energy will be transferred to the light electron component, which is usually the case, but the cluster explosion and ions with energies of hundreds of keV observed in experiments suggest other outcomes are possible. That is why it is instructive to compare the energy deposited into the electron and ion components of the cluster, as well as other possible channels. For clusters with $R_0 < 20$ Å, more than 70% of the absorbed energy is converted into kinetic energy of the electrons [Fig. 3(b)]. This is indeed in accordance with the widely accepted notion that the absorbed energy is transferred to the light electron component. For the smallest clusters considered, the energy deposited in the heavy-particle component (i.e., ions) is ~4 times smaller. But in the opposite case of clusters with initial radius 50–100 Å, the energy is absorbed predominantly by the heavy-particle component. This observation has a practical side, related to particle acceleration and fusion. Large clusters are ideal for heavy ion acceleration and ultimately fusion, since more than 50% of the laser energy can be converted into ion kinetic energy. Regardless of the cluster size, however, ~90% of the absorbed energy ends up as kinetic energy of electrons and ions; the other 10% goes for OFI or remains as potential energy of the system. The energy spent for OFI varies greatly with cluster size: for clusters with initial radius $R_0 = 10$ Å it accounts for ~7% of the energy absorption, while for clusters with initial radius $R_0 = 100$ Å it is negligible.

One of the primary purposes of studying laser-cluster interaction is to use clusters to convert UV laser radiation into x rays. The ideal source would absorb all the laser energy and possess high conversion efficiency into radiation. The first requirement can be readily fulfilled as the absorption efficiency increases with cluster size [Fig. 3(a)], and for clusters with an appropriately chosen number of atoms it approaches unity. Large clusters, however, convert the absorbed energy primarily into kinetic energy of ions [Fig. 3(b)]. These conflicting requirements result in an optimum cluster size. To study the radiation properties of clusters, we estimated the energy emitted as radiation. We assume that every process of electron impact excitation of an ion with an average charge per atom $Z-1$ leads to radiation. The power emitted as radiation from a single cluster is

$$\frac{dE^{\mathrm{rad}}(t)}{dt} \equiv \frac{dE^{\mathrm{exc}}(t)}{dt} = \sum_{k=1}^{N(Z-1)} \sigma_k^{\mathrm{exc}}[E_k(t)]\mathrm{v}_k(t)\Delta E^{\mathrm{exc}}[Z(t)]N/V(t). \quad (2)$$

In Eq. (2), $\sigma_k^{\mathrm{exc}}(E_k)$ is the electron impact excitation cross section of the kth electron with energy E_k and velocity v_k,[18] ΔE^{exc} is the excitation energy of an ion with charge $Z-1$, and $V = \frac{4}{3}\pi R^3$ is the cluster volume. All quantities, including the cluster volume, are time dependent. The summation in Eq. (2) is over all free electrons that reside inside the cluster at time t. The radiation yield

$$\eta^{\mathrm{exc}} = E^{\mathrm{rad}}/E^{\mathrm{abs}}, \quad (3)$$

taken at the end of the laser pulse, is plotted in Fig. 4. For clusters with initial radius $R_0 = 10$ Å, η^{exc} is below 1% since all free electrons are quickly removed from the cluster, resulting in a low excitation rate. With increasing cluster size, the electron impact excitation rate (2) scales approximately as the number of atoms per cluster, while the absorbed energy in the denominator scales as $E^{\mathrm{abs}} \sim N^{5/3}$. Thus the radiation efficiency for large clusters is also low. At a peak laser intensity $I_0 = 10^{16}$ W/cm^2 the optimum initial cluster radius is $R_0 \approx 20$ Å. Apparently, with increasing peak laser intensity this optimum shifts to larger R_0. Indeed, our simulations show that at $I_0 = 10^{17}$ W/cm^2, the optimum initial cluster radius is $R_0 \approx 30$ Å.

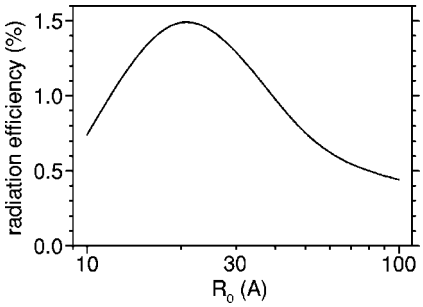

FIG. 4. Radiation efficiency vs initial cluster radius. The conditions are the same as in Fig. 1.

The problem of optimizing the radiation yield is actually more complicated. The cluster size affects the average charge per atom (Fig. 1), which, in turn, leads to radiation from different atomic shells and results in radiation in different spectral ranges. For example, small clusters attain small average charge per atom compared to larger ones and will radiate at longer wavelengths. So optimizing the radiation yield should additionally include consideration of the spectral range of interest. This is the subject of our next investigation, since it requires an atomic physics model, which has detailed energy level structure of the ions under consideration. We are in the process of constructing such a model, and will report the results in a follow-up paper. In general, the resulting spectrum depends on both the cluster size and laser intensity.

The removal of electrons from the cluster, as well as cluster explosion can be visualized by taking snapshots of the particles positions in time. Figure 5 displays the positions of the macroparticles at equally spaced times for a cluster consisting of $N = 6144$ atoms and initial radius $R_0 = 50$ Å. The computations are done in three dimensions, but for convenience the presentation is two dimensional in the XY plane. Each electron macroparticle contains 100 electrons and each ion macroparticle contains 61.4 ions. The average charge per ion versus time is plotted in Fig. 1. The figures to the left refer to electrons, while the figures to the right refer to ions. At $t = 0$ all particles are neutral and reside inside the cluster

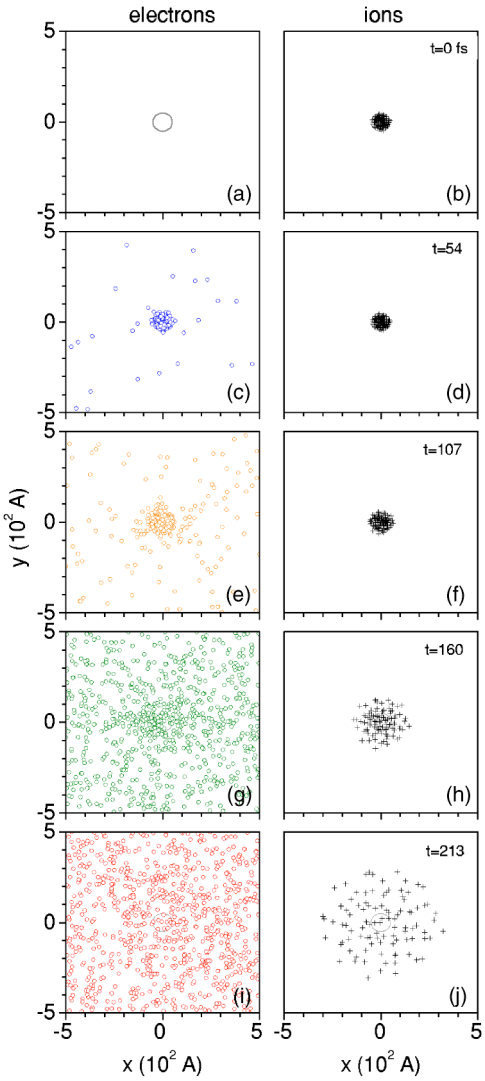

FIG. 5. (Color online) Positions of the macroparticles in the XY plane at different times for a Xe cluster with 6144 atoms/cluster and initial cluster radius $R_0=50$ Å. X is parallel to the laser field and $+Y$ is the direction of propagation. The magnetic field is in the paper. The conditions are the same as in Fig. 1.

[Figs. 5(a) and 5(b)]. Some ~40 fs after the laser is turned on (~160 fs before the peak intensity), the xenon atoms are ionized and a few electrons are created. The electrons in the weakly ionized cluster are exposed to two forces: one from the laser electric field and another due to Coulomb attraction from the ion core. The latter is rather weak and a few energetic electrons leave the cluster. Surprisingly, some electrons can even reach the cluster boundary and join the next cluster [Fig. 5(c)]. Meanwhile the ions remain immobile, as the cluster has not yet absorbed enough energy to cause hydrodynamic expansion [Fig. 5(d)]. A snapshot of the particle positions at a later time [Fig. 5(e)] indicates that more than 50% of the electrons have been removed from the cluster. Fifty femtoseconds later ($t=160$ fs) ~90% of the electrons become outer electrons with significant kinetic energy (~4 keV) filling uniformly the intercluster space [Fig. 5(g)]. At that moment, all prerequisites for cluster explosion are set up and the cluster expands very rapidly. The cluster size is

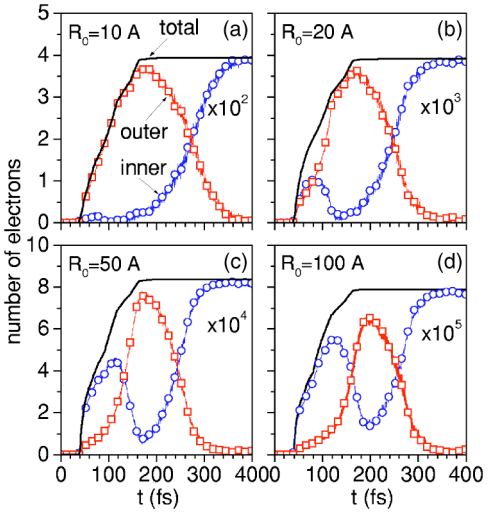

FIG. 6. (Color online) Number of inner electrons, outer electrons, and total number of electrons (solid line) for cluster with $R_0=10$ Å (a), 20 Å (b), 50 Å (c), and 100 Å (d). The conditions are the same as in Fig. 1.

now four times the initial cluster radius [Fig. 5(h)]. The explosion of the ion component progresses, and shortly after the laser intensity goes through maximum, a uniform plasma is formed.

The snapshots in Fig. 5 are very insightful, providing a qualitative picture of the electron dynamics. The processes of ionization and removal of electrons from the cluster can be better understood quantitatively by plotting the number of inner and outer electrons versus time (Fig. 6). The number of inner electrons is a complex function of time resulting from the interplay between ionization, removal of electrons from the cluster and cluster expansion. Initially, the number of inner electrons increases, goes through a maximum, decreases, and then increases again. The initial increase is obviously due to ionization and accumulation of electrons inside the cluster. The removal of electrons from the cluster, conversely, reduces the number of inner electrons and increases the number of outer electrons. The balance between inner and outer electrons is also strongly influenced by a third factor: the cluster expansion. Most electrons leaving the cluster stay in the vicinity of the cluster, and when the cluster expands, they are recaptured. The cluster expansion engulfs electrons continuously, thus increasing the number of inner electrons and decreasing the number of outer electrons. As a result the number of outer electrons goes through a maximum at $t\approx 150-200$ fs, right at the onset of the cluster expansion. At its peak the fraction of outer electrons reaches 80%–90% of the total number of electrons. Near the peak of the laser intensity, the cluster expansion is very fast, and the cluster recaptures outer electrons vigorously. When the cluster radius becomes comparable to the intercluster distance, all outer electrons are recaptured and become inner electrons.

The mean electron energy and density versus time are shown in Fig. 7. The electron density inside the cluster (right) rises quickly due to ionization, goes through a maximum and rapidly decreases. This is typical for clusters of all sizes considered in the present investigation. The maximum electron density is between 10^{21} and 10^{23} cm^{-3} and the de-

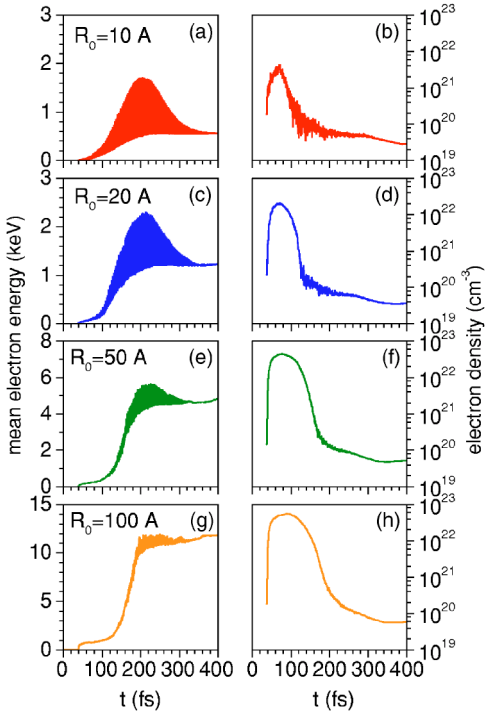

FIG. 7. (Color online) Mean electron energy (left) and density (right) vs time for clusters with $R_0=10$ Å (a), 20 Å (c), 50 Å (e), and 100 Å (g). The conditions are the same as in Fig. 1.

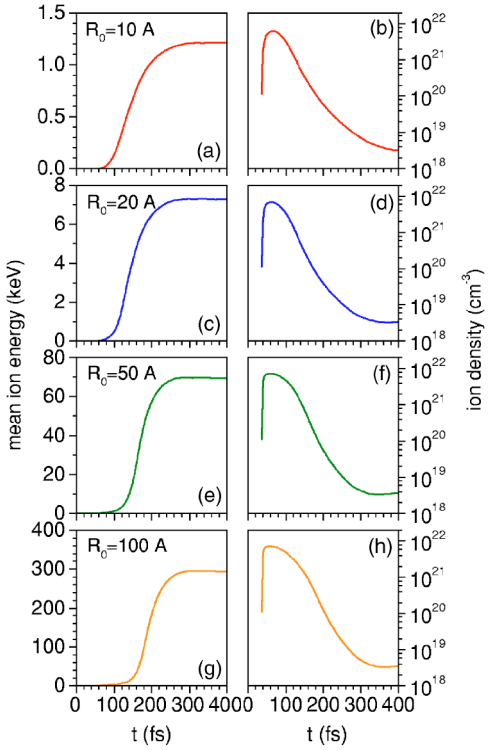

FIG. 8. (Color online) Mean ion energy (left) and density (right) vs time for clusters with $R_0=10$ Å (a), 20 Å (c), 50 Å (e), and 100 Å (g). The conditions are the same as in Fig. 1.

crease of the electron density is due to cluster expansion. Qualitatively, our results agree with predictions from fluid models.[5] The mean electron energy U_e is modulated by the ponderomotive energy that adds a high-frequency component to the slowly time-varying mean electron energy acquired due to inverse bremsstrahlung. For $R_0=10$ Å [Fig. 7(a)] the modulation is substantial since the ponderomotive energy ($U_p \approx 600$ eV) is comparable to the mean electron energy itself. The mean electron energy increases with the cluster size. This is a direct consequence of the nonlinear energy absorption with cluster size, seen in Fig. 3. For clusters with $R_0 > 50$ Å, the modulation of the mean energy is less pronounced compared to clusters with $R_0=10$ Å since $U_p \ll U_e$. In all cases the mean electron energy is in the keV range, sufficient for collisional excitation and ionization. The most intriguing observation is the lack of resonance energy absorption during the so-called plasmon resonance. The plasmon resonance occurs when the electron plasma frequency equals $\sqrt{3}$ times the laser frequency ω during the transition from overdense to underdense plasma and it is manifested by a "spike" of both the mean electron energy and power absorption.[5] We do not observe either (Figs. 2 and 7). Perhaps the reason is the nonuniform electron density, causing the plasmon resonance to exist only locally and for a very short period of time, as surmised in Ref. 6.

The mean ion energy and density versus time are shown in Fig. 8. Their temporal behavior is qualitatively similar for different cluster sizes. The peak ion density is practically the same for all cluster sizes. The magnitude of the mean ion energy, however, increases with cluster size, just like the mean electron energy. This is also a direct consequence of the nonlinear energy absorption with cluster size, and the fact that the absorbed energy is predominantly converted into kinetic energy of ions. The final ion energy is a strongly increasing function of the initial cluster radius. Tenfold increase of the initial cluster radius results in more than a 200 times increase of the mean ion energy. A summary of the

TABLE I. A summary of the average charge per atom, mean electron and ion energies, absorbed energy per atom, and absorbed energy per cluster for clusters with initial cluster radius $R_0=10$, 20, 50, and 100 Å.

Cluster size (Å)	10	20	50	100
Number of atoms per cluster	49	393	6144	4.91×10^{4}
Average charge per atom	8.0	9.9	13.5	16.0
Mean electron energy (keV)	0.67	1.2	4.8	13.1
Mean ion energy (keV)	1.2	7.2	69.4	291
Absorbed energy per cluster (J)	5.2×10^{-14}	1.3×10^{-12}	1.4×10^{-10}	4.1×10^{-9}
Absorbed energy per atom (J)	1.1×10^{-15}	3.2×10^{-15}	2.3×10^{-14}	8.3×10^{-14}

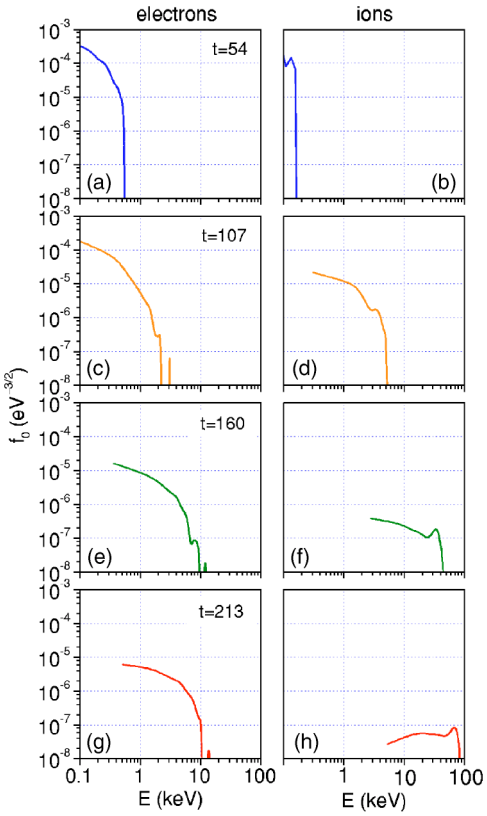

FIG. 9. (Color online) The EEDF (left) and IEDF (right) at different times for a Xe cluster with 6144 atoms/cluster and initial cluster radius R_0 =50 Å. The conditions are the same as in Fig. 1.

mean ion energy for clusters with different number of atoms is given in Table I.

The energy distribution of the particles is of fundamental importance and interest. It can reveal a great deal of information about energy absorption and collisions. The particle simulation model keeps track of each species' position and velocity at any given time and the energy distribution function can easily be constructed. The EEDF and IEDF are the single most important characteristic of the electrons and ions, respectively. We plot a sample EEDF (left) and IEDF (right) for the intermediate cluster size R_0=50 Å (Fig. 9). The low-energy part of the EEDF is Maxwellian, but there is a non-Maxwellian component at high energy. The IEDF is somewhat more complicated and evolves more slowly in time. For the first 50 fs the ions are still "cold," but they gradually pick up energy with increasing the laser intensity. The IEDF goes through several stages, starting as Maxwellian and ending as a flat distribution with a cut-off energy of a hundred keV. This final IEDF, shown in Fig. 9(h) (in units eV$^{-3/2}$), is in agreement with analytical expression and calculations made in Ref. 8. The cluster expansion relative to the initial cluster radius is shown in Fig. 10. The reasons for this expansion are well known[5] and will not be commented on here.

IV. SUMMARY: COMPARISON BETWEEN SMALL AND LARGE CLUSTERS

We studied Xe clusters comprised of different number of atoms, subject to intense laser radiation with a peak laser

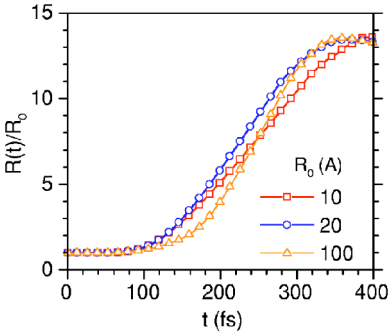

FIG. 10. (Color online) Normalized cluster size R/R_0 vs time for cluster with R_0=10, 20, 100 Å. The conditions are the same as in Fig. 1.

intensity of 10^{16} W/cm^2, using a particle simulation model. The temporal variation of basic cluster properties such as electron and ion positions and velocity, global electron and ion densities, EEDF, IEDF, average charge per ion, absorbed energy, cluster expansion, ionization, and removal of electrons from the cluster was investigated and discussed. Clusters with different sizes exhibit several common features, such as ionization, removal of electrons from the cluster, radiation, and Coulomb explosion. There are, however, profound differences between small and large clusters, which are summarized as follows.

(a) The absorbed energy per cluster increases nonlinearly with the number of atoms per cluster as $N^{5/3}$. As a consequence larger clusters absorb more energy per atom compared to smaller clusters. As observed experimentally, clusters can fully absorb the laser energy.
(b) The energy balance shows that ~90% of the absorbed energy is converted into kinetic energy of electrons and ions. This energy is equally shared between the electron and ion components of the cluster, with prevalence of one or the other depending on the initial cluster radius. This is a very effective method for ion acceleration, since clusters can absorb ~100% of the input laser energy and more than 50% of it can be converted into ion acceleration.
(c) The mean electron and ion energies increase with cluster size as $N^{1/3}$ and $N^{2/3}$, respectively.
(d) The final average charge per atom increases with the number of atoms per cluster due to collisional ionization. The radiation is then expected to shift to shorter wavelengths.
(e) Larger clusters are more advantageous for achieving particle acceleration, while smaller clusters are best suited for radiation production.
(f) Cluster expansion is independent of the cluster size.

ACKNOWLEDGMENTS

This work was supported in part by DARPA and by ONR under the NRL 6.1 program.

APPENDIX: EQUATIONS OF MOTION

The macroparticle trajectory is governed by the relativistic equations of motion

$$\frac{dp_i}{dt} = q_i[E(t) + v_i \times B(t)/c] - \sum_j \nabla \Phi_{ij}, \tag{A1}$$

$$p_i = \gamma_i m_i v_i, \quad \gamma_i = 1/\sqrt{1 - |v_i|^2/c^2}, \tag{A2}$$

$$\frac{dr_i}{dt} = v_i, \tag{A3}$$

where $p_i = p_i(x,y,z)$ is the relativistic momentum, γ_i is the relativistic factor, $r_i = r_i(x,y,z)$, $v_i = v_i(x,y,z)$, m_i, and q_i are the coordinate, velocity, mass, and charge of the ith macroparticle, respectively, $|v_i|$ is the magnitude of the macroparticle velocity, E and B are the externally applied electric and magnetic fields, and Φ_{ij} is the interaction potential between macroparticles i and j, which, in its simplest form is $\Phi_{ij} = q_i q_j/|r_i - r_j|$.

[1] T. Ditmire, J. W. G. Tisch, E. Springate, M. B. Mason, N. Hay, R. A. Smith, J. Marangos, and M. H. R. Hutchinson, Nature (London) **386**, 54 (1997).
[2] T. Ditmire, J. Zweiback, V. P. Yanovsky, T. E. Cowan, G. Hays, and K. B. Wharton, Phys. Plasmas **7**, 1993 (2000).
[3] A. McPherson, B. D. Thompson, A. B. Borisov, K. Boyer, and C. K. Rhodes, Nature (London) **370**, 631 (1994).
[4] A. B. Borisov, X. Song, F. Frigeni, Y. Koshman, Y. Dai, K. Boyer, and C. K. Rhodes, J. Phys. B **36**, 3433 (2003).
[5] T. Ditmire, T. Donnelly, A. M. Rubenchik, R. W. Falcone, and M. D. Perry, Phys. Rev. A **53**, 3379 (1996).
[6] H. M. Milchberg, S. J. McNaught, and E. Parra, Phys. Rev. E **64**, 056402 (2001).
[7] E. Parra, I. Alexeev, J. Fan, K. Y. Kim, S. J. McNaught, and H. M. Milchberg, J. Opt. Soc. Am. B **20**, 118 (2003).
[8] I. Last and J. Jortner, J. Chem. Phys. **120**, 1336 (2004); **120**, 1348 (2004); **121**, 3030 (2004).
[9] I. Last and J. Jortner, Phys. Rev. A **62**, 013201 (2000).
[10] I. Last and J. Jortner, Phys. Rev. A **60**, 2215 (1999).
[11] M. Eloy, R. Azambuja, and J. T. Mendonca, and R. Bingham, Phys. Plasmas **8**, 1084 (2001).
[12] M. Eloy, R. Azambuja, and J. T. Mendonca, and R. Bingham, Phys. Scr., T **T89**, 60 (2001).
[13] P. Greschik and H.-J. Kull, Laser Part. Beams **22**, 137 (2004).
[14] T. Taguchi, T. M. Antonsen, Jr., and H. M. Milchberg, Phys. Rev. Lett. **92**, 205003 (2004).
[15] D. Bauer, Appl. Phys. B **78**, 801 (2004).
[16] D. Bauer, J. Phys. B **37**, 3085 (2004).
[17] G. M. Petrov, J. Davis, A. L. Velikovich, P. C. Kepple, A. Dasgupta, R. W. Clark, A. B. Borisov, K. Boyer, and C. K. Rhodes, Phys. Rev. E **71**, 036411 (2005).
[18] H. W. Drawin, Z. Phys. **225**, 483 (1969).